LAWRENCE
LIVERMORE
NATIONAL
LABORATORY

LLNL-PROC-403213

Dust Measurements in Tokamaks

D.L. Rudakov, J.H. Yu, J.A. Boedo, E.M. Hollmann, S.I. Krasheninnikov, R.A. Moyer, S.H. Muller, A. Yu, M. Rosenberg, R.D. Smirnov, W.P. West, R.L. Boivin, B.D. Bray, N.H. Brooks, A.W. Hyatt, C.P.C. Wong, M.E. Fenstermacher, M. Groth, C.J. Lasnier, A.G. McLean, P.C. Stangeby, S. Ratynskaia, A.L. Roquemore, C.H. Skinner, W. M. Solomon

April 25, 2008

17th High Temperature Diagnostics Conference
Albuquerque, NM, United States
May 11, 2008 through May 15, 2008

Disclaimer

This work performed under the auspices of the U. S. Department of Energy by Lawrence Livermore National Laboratory under Contract DE-AC52-07NA27344.

Dust Measurements in Tokamaks

D.L. Rudakov, J.H. Yu, J.A. Boedo, E.M. Hollmann, S.I. Krasheninnikov, R.A. Moyer, S.H. Muller, A.Yu. Pigarov, M. Rosenberg, R.D. Smirnov

University of California, San Diego, California 92093 USA

W.P. West, R.L. Boivin, B.D. Bray, N.H. Brooks, A.W. Hyatt, C.P.C. Wong

General Atomics, P.O. Box 85608, San Diego, California 92186-5608 USA

M.E. Fenstermacher, M. Groth, C.J. Lasnier

Lawrence Livermore National Laboratory, Livermore, California 94550 USA

A.G. McLean, P.C. Stangeby

University of Toronto Institute for Aerospace Studies, Toronto, Ontario, Canada M3H 5T6

S. Ratynskaia

Space and Plasma Physics, EE, Royal Institute of Technology, SE-10044 Stockholm, Sweden

A.L. Roquemore, C.H. Skinner, W.M. Solomon

Princeton Plasma Physics Laboratory, Princeton, New Jersey 08543 USA

Abstract. Dust production and accumulation impose safety and operational concerns for ITER. Diagnostics to monitor dust levels in the plasma as well as in-vessel dust inventory are currently being tested in a few tokamaks. Dust accumulation in ITER is likely to occur in hidden areas, e.g. between tiles and under divertor baffles. A novel electrostatic dust detector for monitoring dust in these regions has been developed and tested at PPPL. In DIII-D tokamak dust diagnostics include Mie scattering from Nd:YAG lasers, visible

imaging, and spectroscopy. Laser scattering resolves size of particles between 0.16–1.6 μm in diameter; the total dust content in the edge plasmas and trends in the dust production rates within this size range have been established. Individual dust particles are observed by visible imaging using fast-framing cameras, detecting dust particles of a few microns in diameter and larger. Dust velocities and trajectories can be determined in 2D with a single camera or 3D using multiple cameras, but determination of particle size is problematic. In order to calibrate diagnostics and benchmark dust dynamics modeling, pre-characterized carbon dust has been injected into the lower divertor of DIII-D. Injected dust is seen by cameras, and spectroscopic diagnostics observe an increase of carbon atomic, C_2 dimer, and thermal continuum emissions from the injected dust. The latter observation can be used in the design of novel dust survey diagnostics.

PACs Nos.

I. INTRODUCTION

Dust is commonly found in magnetic fusion devices (see [1-7] and references therein). In the contemporary machines dust is generally of no great concern. However, dust generation in the next-step devices is expected to increase by several orders of magnitude due to the increased duty cycle and higher magnitude of particle and power fluxes deposited on the plasma facing components (PFCs). Dust production and accumulation may impose serious safety and operational concerns for the International Thermonuclear Experimental Reactor (ITER) by contributing to tritium inventory rise and leading to radiological and explosion hazards. In ITER dust accumulation is a licensing issue with in-vessel inventory limits for C, Be and W dust of 200, 100, and 100 kg, respectively. Furthermore, amount of dust on hot surfaces is limited to 6 kg for each species. Projections of dust production and accumulation rates based on experience from existing devices are needed. In addition, dust penetration of the core plasma can cause undesirably high impurity concentration and degrade performance, thus studies of the dust transport and dynamics are also quite important.

Dust particulates found in tokamaks and other fusion devices range in size between ~10 nm and a few hundred μm [1, 3-7]. Chemical composition of the dust is determined by the PFC materials. Dust production mechanisms in tokamaks with carbon-based PFCs include flaking of redeposited layers, brittle destruction of graphite, arcing, agglomeration from supersaturated vapor, and growth from hydrocarbon molecules [6]. Disruptions, large Edge Localized Modes (ELMs) and other transient events result in increased dust production [5,7].

Dust diagnostic techniques are not yet adequately developed to make quantitative predictions for the next step devices. However, some progress has been made in recent years. In Section II we will give a brief review of the dust diagnostic techniques currently employed in tokamaks and stellarators and those proposed for the next step devices. Then in Section III we will discuss in more detail dust diagnostics and dust measurements on DIII-D tokamak and possible extension of those techniques for the future devices.

II. DUST MEASUREMENTS IN EXISTING TOKAMAKS AND DIAGNOSTICS PROPOSED FOR THE NEXT-STEP DEVICES

Dust diagnostics can be loosely divided into two groups: (A) diagnostics of dust on surfaces and (B) diagnostics of dust in plasma. Group (A) diagnostics are ultimately more important for the next-step devices since they are directly related to monitoring the in-vessel dust inventory. Group (B) diagnostics should be pursued in the contemporary machines since they can provide insight into dust production mechanisms and dust transport.

A. Diagnostics of dust on surfaces

Collection techniques have been used for years to study dust accumulation in fusion devices [3,5]. Samples collected during entry vents allow to determine dust size distribution, chemical composition, and estimate the in-vessel dust inventory. However, this technique typically provides information averaged over months of operations and thousands of plasma discharges, so correlating dust production and accumulation rates with the discharge parameters is hardly possible.

Electrostatic detectors [8-10] offer promising new approach to monitoring conductive dust in hard-to-access areas, where dust accumulation is likely to occur in the next-step devices. The device consists of two closely interlocking grids of wires on a circuit board (Fig. 1). A few prototype devices have been fabricated and tested in laboratory with encouraging results. Tests have also been performed in the NSTX tokamak, but the dust levels proved out to be too low for conclusive results. The estimated sensitivity of the prototype devices is a few tens of ng/cm^2/count [10], which is not quite sufficient for contemporary tokamaks, but more than adequate for ITER. Additional benefit of electrostatic detectors is that they eject or evaporate most of the incident dust [9], and can therefore keep surfaces essentially dust-free.

Capacitive diaphragm microbalance [11,12] is another promising approach for monitoring of the dust accumulation in the next-step devices. It's based on pressure gage technology and is suitable for use in a tokamak environment. Prototype device has been tested in laboratory, where a sensitivity of 500 μg/cm^2 and dynamic range of at least 10^3 were demonstrated [12].

IR thermography can detect dust presence on hot PFC surfaces [13]. This may be an valuable tool for complying with a strict limit for dust on hot surfaces in ITER.

Laser-induced breakdown spectroscopy can be used to locally ablate dust deposited on a surface and determine its chemical composition [14]. However, relating the information obtained with this diagnostic to the quantity of the dust is non-trivial.

Doped PFCs for exact erosion measurements have been proposed as an alternative approach to monitoring levels of dust and debris in ITER [11]. While this technique would allow estimating the upper limit of the in-vessel dust inventory, it can't completely

substitute for dust diagnostics, since it would tell nothing about what fraction of eroded material is turned into dust and where the dust is accumulated.

B. Diagnostics of dust in plasma

2D imaging [2,4,15,16] allows recording individual particle trajectories and estimating the particle velocities. However, particle size is hard (if at all possible) to determine. Standard frame rate cameras generally have poor contrast ratio for moving objects against the background and can therefore detect only large particles. Fast-framing or gated cameras can resolve smaller, faster moving particles. Use of multiple cameras with intersecting views allows unfolding particle trajectories in full 3D [15,16]. This capability is invaluable for benchmarking dust dynamics codes such as Dust3D [7].

Scattering techniques rely on detection of laser light scattered by dust particles within a plasma [17-19]. They allow estimating size of small particles (comparable to or smaller than the laser wavelength) and measuring dust size distributions and dust density in the plasma. Dust observation rates are generally low, so statistical analysis of the data is required. If the laser beam intensity is high, dust particles can be ablated by the beam, so modeling of the dust-beam interaction is required. Measurements of dust by Mie scattering in DIII-D [18,19] will be discussed in Section III.

Spectral survey diagnostics generally do not resolve individual dust particles, but can provide indications of dust presence in a plasma. Combined survey of impurity lines and thermal continuum radiation is proposed for dust detection (see Section III).

Laser-induced incandescence [20,21] is used for dust measurements in processing plasmas. Particle size and possibly concentration can be determined. Although low dust densities ($<< 1$ cm^{-3}) in the contemporary tokamak plasmas preclude the use of this

technique, it may prove suitable for dust measurements in the far scrape-off layer (SOL) and remote divertor regions of the next-step devices.

Langmuir probes can be sensitive to dust provided the dust velocity is sufficiently high. Recent work at FTU tokamak provided evidence of hyper-velocity (at or above 10 km/s) dust presence [22,23]. Signals measured by a probe in the outboard SOL were shown to be consistent with dust particles hitting the probe tip and causing evaporation and ionization of the tip material [23]. Craters observed on the surface of the probe tip upon extraction (see Fig. 2) are also consistent with the above picture and hard to explain otherwise. However, so far no other machine has reported presence of hyper-velocity dust.

Injection of pre-characterized dust into plasma [17,24] can be used for diagnostic calibration and benchmarking of modeling. In addition, the dust itself can serve as a diagnostic of the SOL plasma flows. Experiments with injected dust in DIII-D are described in the following section.

III. DUST MEASUREMENTS IN DIII-D TOKAMAK

DIII-D [25] is a tokamak with major and minor radii of 1.67 m and 0.67 m, and all-carbon (graphite) PFCs. It has two poloidal divertors and can be operated in lower single null (LSN), upper single null (USN), double null (DN) and wall-limited magnetic configurations. Arrangement of the diagnostics used for dust detection in DIII-D is shown in Fig. 3. Shaded areas represent camera views: 1 – fast framing camera, 2 – tangential divertor TVs, 3 – DiMES TV. Dots in (a) show views of spectroscopic diagnostics: 4 – MDS spectrometer [26], 5 – filterscopes (telescopes with line filters

coupled to photomultipliers) [27]. MDS lines of view are shown in (b). Outermost viewing volumes of the core (6) and divertor (7) Thomson scattering systems are marked in (b). Location of the divertor material evaluation station (DiMES) (8) that allows insertion of material samples in the lower divertor [28] is marked in (a) and (b). Poloidal cross-section of a last closed flux surface (LCFS) of a LSN equilibrium with DiMES in the private flux region is shown in (b).

Thomson scattering system based on 8 ND:YAG lasers is used primarily for the measurements of the electron density and temperature profiles [29]. Each laser produces pulses of about 10 ns duration at a 20Hz repetition rate with a total energy per pulse of 0.5 J. Vertical core system has 4 collinear lasers, divertor system has a single laser. The laser beam has a center region of high intensity (above 10^{12}Wm^{-2}) 3 mm in diameter, surrounded by a halo region with about 5% of the center intensity that extends out to a diameter of 5 mm [18]. Light scattered from multiple positions along the laser path inside the plasma is collected by an optical system located outside the vacuum vessel and directed to polychromators. The viewing volumes are typically 1 cm in height and 5 mm in diameter. Each polychromator has 6 detectors at different wavelengths. Non-shifted detector channels at the laser wavelength of 1064 nm allow for detection of light scattered by the dust particles. Signals from large particles cause saturation of the non-shifted channels, but some of them can be resolved by detectors with narrow band filters centered at 1062 nm which have extinction factor for the laser wavelength of ~10^{-2}. More detail on the dust detection by the Thomson scattering system is available in Ref. [18].

Because of the short laser pulse duration and small viewing volume dust observation rates are low, a few events per discharge or less. Nevertheless, statistical analysis of the

data provides an estimate of the total dust content in the edge and SOL plasmas and allows establishing trends in the dust production rates. Dust size can be estimated from the amplitude of the detected scattered signal. Initial estimates using Rayleigh model has put resolved size within the range between 50–250 nm [18]. However, Rayleigh approximation is marginal for the larger particles. Another complication in the data interpretation arises from the laser beam energy being sufficient to partially or even completely evaporate smaller particles. A more accurate analysis using Mie scattering model and taking account of the particle ablation by the laser has put the detectable particle size within the range of 0.16–1.6 μm in diameter [19]. Probability distribution functions (PDFs) of the radii of experimentally detected dust particles are shown in Fig. 4(a). The PDFs were constructed from a fit to the scattering signal distribution obtained over 710 discharges comprising 1580 dust events [18] assuming graphite particles with complex index of refraction m = 3.33-i2.07 [19]. The dashed line is obtained assuming the detected particles were in the center region of the beam, and the solid line is obtained assuming the particles were in the halo region. For smaller particles ($R < 0.2$ μm), the slope of the PDF is close to R^{-3}, while for larger particles it is smaller. Therefore, the contribution of large particles to the total dust mass is larger than of small ones despite the much larger number density of small particles. Figure 4(b) shows measured dust density profiles in low confinement (L-) and high confinement (H-) modes. The dust density is barely above the detection limit at the LCFS and increases with distance into the SOL. It is higher in H-mode that has higher heating power and ELMs causing more intense plasma-wall interaction. However, even at the highest dust densities measured and with the dust size determined using Mie model, estimated total carbon content of the

dust is less than a few percent of the plasma carbon impurity content. Therefore, submicron dust is not a major impurity source in DIII-D.

Larger dust particles are detected by optical imaging with cameras. A few standard frame rate CMOS and CID cameras and a fast framing CMOS camera are available on DIII-D (Fig. 3). A tangential view of the lower divertor (view (2) in Fig.3) is split between two 60 fields/s CID cameras ("tangential TVs"). Spatial resolution of both tangential TVs is about 1.5–2 cm. A 60 fields/s CMOS camera ("DiMES TV") views vertically down into the lower divertor (view (2) in Fig.3) with a spatial resolution of about 1.5 mm. A fast framing CMOS camera, Phantom 7.1, has a tangential view of the outboard chamber wall (view (1) in Fig.3). The camera has framing rate of up to 26000 frames/s at 256×256 pixel resolution. All cameras have remotely changeable filters. Dust particles are occasionally observed with line filters such as D_α, CIII, etc, but most dedicated dust observations are performed either in full light or with Kodak Wratten 89B infrared filters, which block wavelengths below 700 nm. As noted in Section II, fast camera has inherently higher contrast ratio for moving incandescent objects, and therefore can resolve smaller particles than the standard rate cameras. As a result, dust observation rate of the fast camera is much higher than that of the standard cameras.

During "normal operations", i.e. when the vacuum vessel walls are well conditioned and there are no major disruptions, dust observation rates are low. Standard cameras register only isolated dust events, single numbers per discharge or none, while the fast camera typically observes between 10-100 events per discharge. Individual particles moving at velocities of up to ~500 m/s and breakup of larger particles into pieces are observed. A sequence of frames in Fig. 5 shows a comparatively large (probably tens of

microns in size) and slow (~10 m/s) dust particle marked by an arrow in (a) that first becomes visible in the outboard SOL, moves towards the separatrix (b), then slows down (c), changes direction (d), and finally breaks into 3 smaller particles (e-h). The data were taken by the fast camera in full light, at 2000 frames/s with 497 μs exposure per frame. The total time between frames (a) and (h) is ~60 ms, time between individual frames varies between 8-10 ms.

Disruptions often generate significant amounts of dust which is directly observed by the fast-framing camera. An image of dust produced by a disruption is shown in Fig. 6(a). A single disruption produces up to ~10000 dust particles. Increased dust levels are also observed following entry vents. In the first 2-3 plasma discharges after an entry vent, standard rate cameras detect hundreds of particles and fast camera detects thousands of particles in each discharge. An example of dust tracks observed by DiMES TV viewing the lower divertor from above (view (3) in Fig. 3) is shown in Fig. 6(b). After about 15 discharges dust is virtually gone during the stationary portion of a discharge, and appears at much reduced levels during the plasma initiation and termination phases. After a few days of plasma operations (about 70 discharges) dust levels are further reduced to the "normal operations" rates.

In principle, if the dust chemical composition and the local plasma parameters at the location of a dust particle are known, one can relate the intensity of the thermal radiation from a particle to the particle size [7,30]. Then if an absolute *in situ* calibration of the camera sensitivity is available, it may be possible to determine the particle size from the camera measurements. However, in practice this task is extremely complicated. Luminosity of a dust particle is a very strong function of the local plasma density, n_e, and

electron temperature, T_e [7,30]. Since gradients of n_e and T_e with typical e-folding lengths of 2-8 cm exist in the SOL [31], with a 2D view it's practically impossible to determine a particle position with sufficient accuracy for a reasonable size estimate. This complication may be alleviated if multiple cameras with intersecting views are used to determine the particle position in 3D. However, even the accuracy of ±4 cm achieved in the main chamber SOL of NSTX [15] is at best marginal for a particle size estimate from brightness. Moreover, at least in the "near SOL" within a few cm of the separatrix, where n_e and T_e are sufficiently high to cause significant ablation of a particle surface, radiation from dust particles observed by cameras is not entirely thermal. Line radiation from the ablation cloud around a particle can contribute significantly to or even dominate the detected radiation. In fact, even though the projection area of a single pixel of a fast camera into DIII-D SOL plasma is ~5-10 mm (depending on the location), most observed particles appear as multi-pixel images. It is probably the size of the ablation cloud that defines the image size. This is illustrated in Fig. 5(c), where a large particle clearly develops an ablation cloud appearing as a bright halo elongated along the magnetic field lines.

Injections of pre-characterized dust from a known location can be used to calibrate diagnostic measurements and benchmark modeling of the dust dynamics and transport. Migration of carbon dust was studied in DIII-D by introduction of micron-size (~6 μm median diameter) graphite dust in the lower divertor [24]. A DiMES sample holder filled with ~30 mg of dust was exposed to high-power LSN ELMing H-mode discharges with strike points swept across the divertor floor. In the early part of the discharge the holder with dust was in the private flux region (as shown in Fig. 3(b)), then the outer strike point

(OSP) was swept radially inward over the dust. Following a brief exposure (~0.1 s) at the OSP, part of the dust was injected into the plasma. A frame from the tangential divertor TV (view (2) in Fig. 3) with IR filter shows a direct view of the injection (Fig. 7(a), DiMES location marked by a circle). About 1.5%-2% of the total dust carbon content (2-3×10^{19} carbon atoms, equivalent to a few million dust particles) penetrated the core plasma, raising the core carbon density by a factor of 2–3 and resulting in a twofold increase of the total radiated power. Individual dust particles were observed moving at velocities of 10–100 m/s, predominantly in the toroidal direction for deuteron flow to the outer divertor target, consistent with the ion drag force. The observed velocities and trajectories of the dust particles are in qualitative agreement with modeling by the DustT code [7,30], which solves equations of motion for dust particles in 3D self-consistently using a plasma background from the UEDGE code. The fast framing camera observed large amounts of injected dust in the outboard SOL (Fig. 7(b)), thus confirming DustT prediction that dust can migrate from the lower divertor into the main chamber [30]. An injection of diamond dust of finely calibrated size between 2-4 microns was recently performed. Dust from injection was observed by the fast camera, but requited digital background subtraction to be resolved. Therefore, it was experimentally demonstrated that 4 micron dust is about the smallest that can be resolved by the fast camera in the existing setup at DIII-D.

Filterscopes and MDS spectrometer can't resolve individual dust particles, but may give indications of the dust presence. Figure 8 shows MDS spectra taken at DiMES location before (upper trace) and after (lower trace) the diamond dust injection. Following the injection, strong increase in the thermal continuum emission (appearing as

a constant offset of the upper trace in Fig. 8) is observed. Concurrent increases in CI atomic emission (three distinct peaks observed in both traces) and C_2 dimer emission (wide band of narrow lines, the so-called Swan band) were also observed. This observation may be useful for designing novel survey diagnostics for carbon dust in tokamak divertor and SOL plasmas. Increase in the local thermal continuum emission accompanied by increases in atomic and molecular C radiation can be interpreted as a signature of the dust presence. An array of optical fibers coupled to detectors with appropriate set of filters can provide a relatively inexpensive way of dust monitoring.

IV. DISCUSSION AND SUMMARY

Dust diagnostics in the contemporary tokamaks are still in an early development stage, and considerable progress has to be made to meet the challenges in a next-step device such as ITER. However, progress has been recently made. Prototypes of surface dust diagnostics suitable for use in ITER have been fabricated and tested in laboratory. Various diagnostics of dust in plasmas have been tested in tokamaks with encouraging results, yet there is still considerable space for improvement. For example, scattering diagnostic in DIII-D would benefit from an increased laser beam diameter, eliminating dust ablation by the beam, reducing detector saturation, and increasing the dust observation rate. Intensified fast framing cameras would allow detection of smaller faster particles. Spectral survey diagnostics with appropriate filters could provide a way to monitor dust production rates at multiple locations. Some techniques may be borrowed from other. For example, Aerogel [32] used by STARDUST spacecraft to capture comet particles has been proposed for capturing hyper-velocity dust particles in a tokamak.

Acknowledgments

This work performed under the auspices of the U.S. DOE by LLNL under Contract DE-AC52-07NA27344, DE-AC02-76CH03073, and DE-AC04-94AL85000.

References

[1] R. Behrisch et al., J. Nucl. Mater. **76–77** (1978) 437.

[2] D.H.J. Goodall, J. Nucl. Mater. **111–112** (1982) 11.

[3] W. J. Carmack, *et. al.*, Fusion Eng. Des. **51–52** 477 (2000).

[4] M. Rubel, *et. al.*, Nucl. Fusion **41**, 1087 (2001).

[5] G. Federici, *et. al.*, Nucl. Fusion **41**, 1967 (2001).

[6] J. Winter, Plasma Phys. Control. Fusion **46** B583 (2004).

[7] A. Yu. Pigarov, *et. al.*, Phys. Plasmas **12**, 122508 (2005).

[8] C.H. Skinner, *et. al.*, Rev. Sci. Instrum. **75** 4213 (2004).

[9] C.V. Parker, *et. al.*, J. Nuclear Mater., **363–365** 1461 (2007).

[10] C.H. Skinner, *et. al.*, J. Nuclear Mater., in press (2008).

[11] G. F. Counsell and C. H. Wu, Phys. Scr., T **T91**, 70 (2001).

[12] G. F. Counsell, *et. al.*, Rev. Sci. Instrum. **77** 093501 (2006).

[13] R. Reichle, *et. al.*, J. Nucl. Mater. **290-293** 701 (2001).

[14] G. T. Razdobarin, *et. al.*, Fusion Sci. Technol. **41** 32 (2002).

[15] A.L. Roquemore, *et. al.*, J. Nucl. Mater. **363–365** 222 (2007).

[16] W. Boeglin, *et. al.*, these proceedings.

[17] K. Narihara *et al.,* Nucl. Fusion **37** 1177 (1997).

[18] W. P. West, *et. al.*, Plasma Phys. Control. Fusion **48** 1661 (2006).

[19] R. D. Smirnov, *et. al.*, Plasma Phys. Control. Fusion **49** 347 (2007).

[20] W. W. Stoffels, *et. al.*, J. Vac. Sci. Technol. A **14** 588 (1996).

[21] G. S. Eom, *et. al.*, Appl. Phys. Lett. **83** 1261 (2003).

[22] C. Castaldo, *et. al.*, Nucl. Fusion **47** L5 (2007).

[23] S. Ratynskaia, *et. al.*, Nucl. Fusion **48** 015006 (2008).

[24] D. L. Rudakov, *et. al.*, J. Nuclear Mater. **363–365** 227 (2007).

[25] J. L. Luxon, Nucl. Fusion **42** 614 (2002).

[26] N.H. Brooks, *et. al.*, Rev. Sci. Instrum. **63** 5167 (1992).

[27] R.J. Colchin, *et.al.*, Rev. Sci. Instrum, **74** 2068 (2003).

[28] C.P.C.Wong, *et. al.*, J. Nucl. Mater. **258-263** 433 (1998).

[29] T. N. Carlstrom, *et. al.*, Rev. Sci. Instrum. **63** 4901 (1992).

[30] R. D. Smirnov, *et. al.*, Plasma Phys. Control. Fusion **49** 347 (2007).

[31] D.L. Rudakov, *et. al.*, Nucl. Fusion **45** 1589 (2005).

[32] http://stardust.jpl.nasa.gov/photo/aerogel.html.

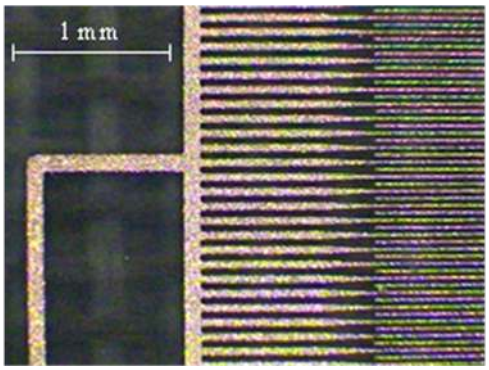

Fig. 1. Electrostatic dust detector.

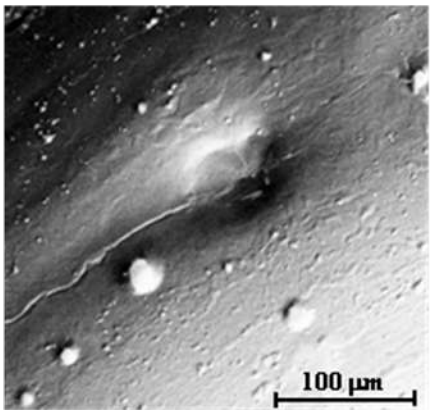

Fig. 2. Crater formed on a surface of a molybdenum probe tip presumably by a hyper-velocity dust impact.

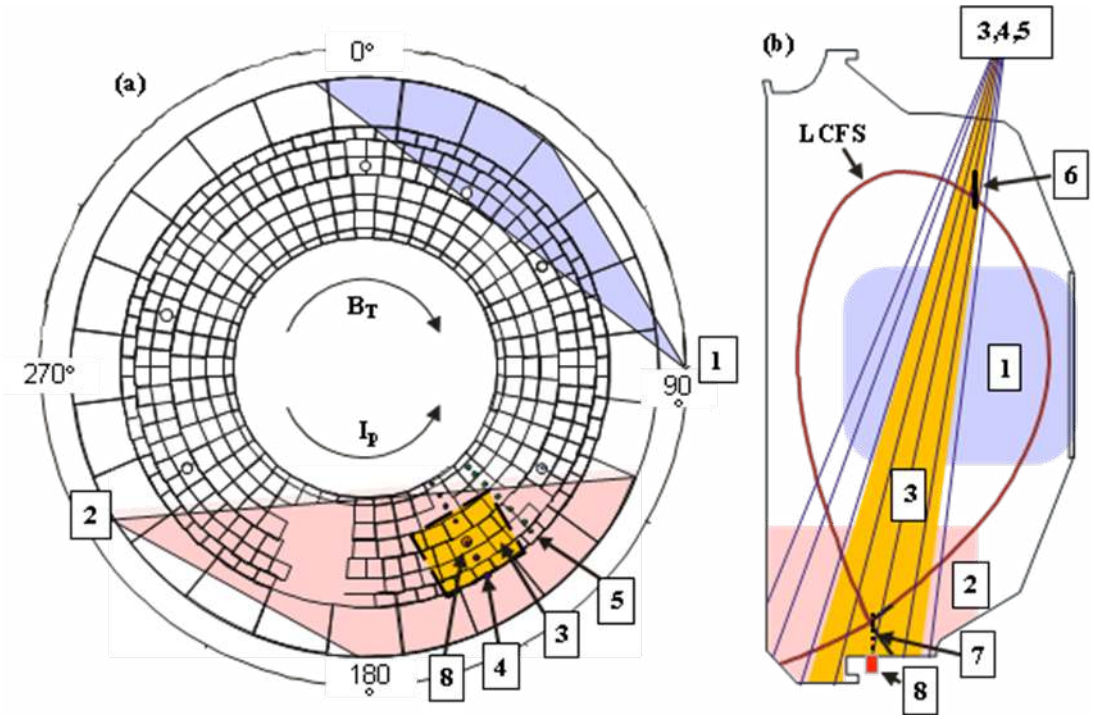

Fig. 3. Diagnostic arrangement on DIII-D: 1 – fast camera, 2 – tangential divertor TVs, 3 – DiMES TV, 4 – MDS, 5 – filterscopes, 6 – core Thomson, 7 – divertor Thomson, 8 – DiMES.

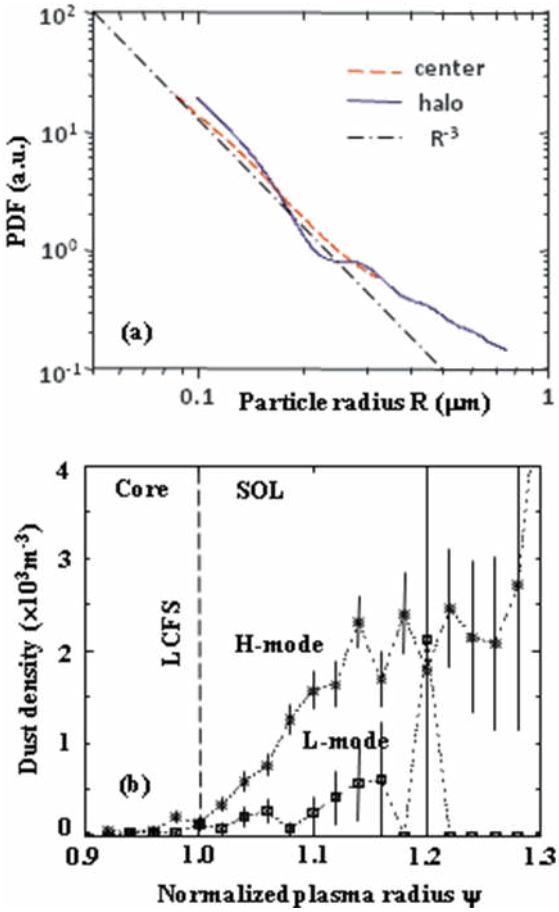

Fig. 4. Dust size distribution (a) and radial density profile (b) measured by Mie scattering in DIII-D.

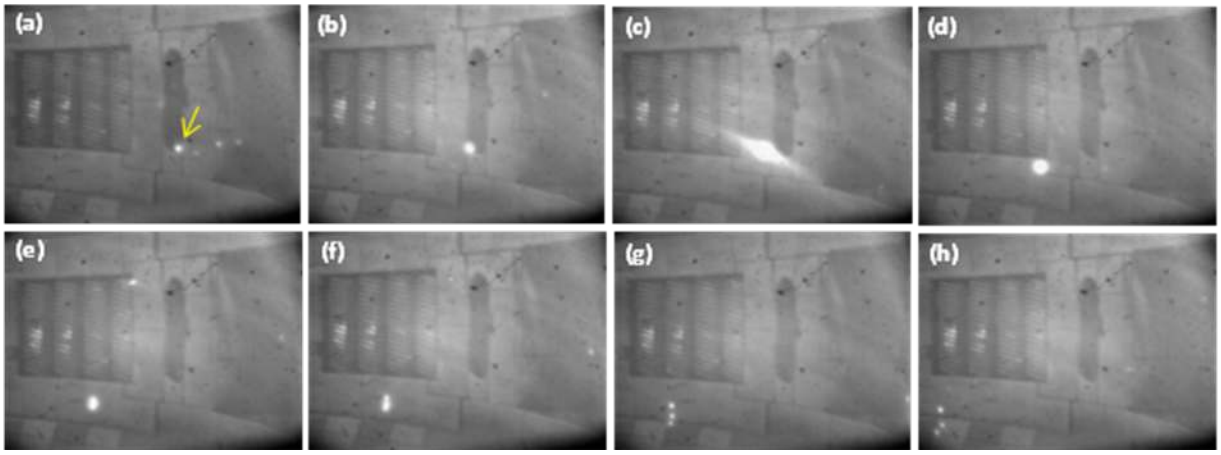

Fig. 5. Time history of a dust particle observed by the fast camera in DIII-D SOL.

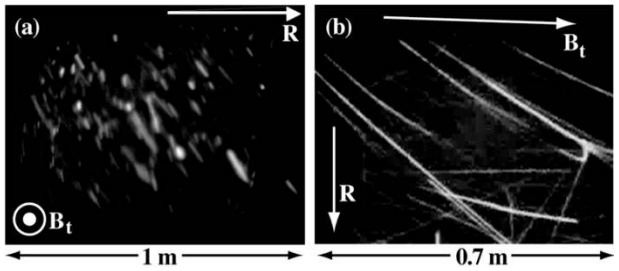

Fig. 6. Dust in DIII-D: (a) dust produced by a disruption (fast camera, tangential view of outboard SOL); (b) dust observed after an entry vent (DiMES TV, looking down in the lower divertor)

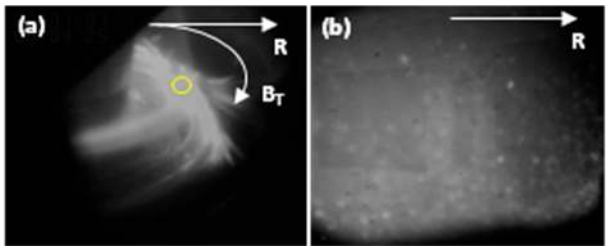

Fig. 7. Injected carbon dust in DIII-D observed in divertor by tangential TV (a) and in the SOL by the fast framing camera (b).

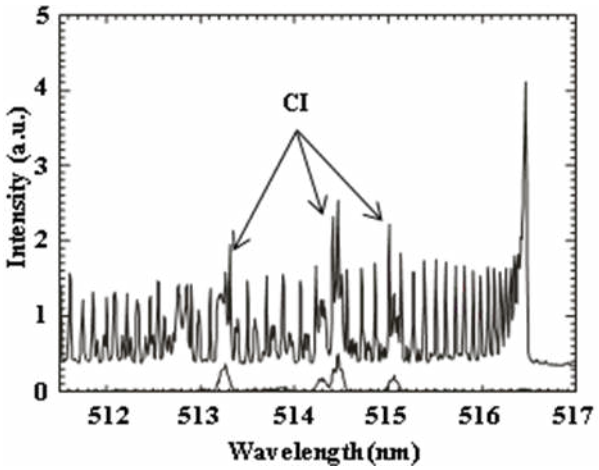

Fig. 8. MDS spectra of CI atomic and C_2 dimer radiation before (lower trace) and after (upper trace) diamond dust injection. Thermal continuum radiation appears as a constant offset of the upper trace.